Homoclinic bifurcation in Blasius boundary-layer flow

Uwe Ehrenstein
Université Lille I, Laboratoire de Mécanique de Lille, URA CNRS 1441, Bd. P. Langevin, F-59655 Villeneuve d'Ascq Cedex, France

Werner Koch
DLR Institut für Strömungsmechanik, Bunsenstr.10, D-37073 Göttingen, Germany

(Received 28 September 1994; accepted 3 March 1995)

In an attempt to elucidate the laminar/turbulent transition mechanism in a Blasius boundary-layer flow, a nonsemisimple resonance of phase-locked secondary instability modes is investigated. The *local* nonlinear behavior is described by means of a center manifold reduction. The numerically computed normal form is of the symmetric Takens–Bogdanov type and predicts a homoclinic orbit which is possibly related to a physical bursting process. A *global* continuation procedure for equilibrated three-dimensional (3-D) waves in the full Navier–Stokes system validates some of the local predictions and very closely outlines the experimentally observed skin friction domain including subcritical transition. © *1995 American Institute of Physics.*

I. INTRODUCTION

The question of a possible link between turbulent fluid flow and low-dimensional dynamics has been explored extensively during recent years. One hopes that low-dimensional models capture the main features of the flow and elucidate more readily the relevant laminar/turbulent transition scenario or provide a deeper understanding of the turbulence generating mechanism. Most of the previous work in this area deals with "closed" flow systems, such as Taylor–Couette or convection problems (see, for example, Refs. 1 and 2 and references cited therein).

One of the first attempts to establish a rational relationship between a turbulent "open" flow system and low-dimensional dynamical systems appears to be the work of Aubry *et al.*[3,4] and Zhou and Sirovich.[5] These authors derived a low-dimensional model by expanding the known velocity field (obtained either experimentally or numerically) in terms of Karhunen–Loève eigenfunctions and truncating at low order. These Karhunen–Loève eigenfunctions are obtained by the so-called proper orthogonal decomposition technique, which is optimal in the sense that the series for the velocity field converges optimally fast by well-defined criteria. While serious controversies still exist with regard to the correct modeling (cf. Berkooz *et al.*,[6] Sirovich and Zhou[7]), both research groups find intermittent and chaotic bursting behavior in their models.

Using direct numerical simulation data of Rist and Fasel,[8] Rempfer and Fasel[9] applied the proper orthogonal decomposition to a transitional flat plate boundary layer which is also at the center of our interest. They were able to demonstrate that the most energetic Karhunen–Loève eigenfunctions are indeed related to observed "coherent structures" and at the same time provide an unambiguous mathematical formulation of the latter. In particular, Rempfer and Fasel[9] identified a higher-order structure during which the spike stage induces a strong updraft away from the wall. As pointed out by the authors, this striking similarity to the bursting event of fully turbulent boundary layers suggests similar underlying mechanisms. More light could be shed on these mechanisms by applying the methods of dynamical systems theory to the truncated evolution equations, as, for example, in Aubry *et al.*[3,4] While such an investigation is planned for the future by the authors, we use in the present paper an alternative method for deriving a low-dimensional model built upon successive bifurcations of the flow. In particular, Guckenheimer and Holmes[10] and Coullet and Spiegel[2] observed that multiple bifurcation points often provide organizing centers for the dynamics of the problem. A local nonlinear analysis leads to so-called normal form or amplitude equations which frequently capture the main features of the full system in a sufficiently large neighborhood of the degeneracy. A major task remains finding the flow conditions which correspond to such multiple bifurcation points. In general, only one primary instability mode can become unstable. Therefore, at the primary instability level, it is customary to add additional control parameters, such as density or concentration gradients, rotation or magnetic fields, to create multiply unstable systems, which can then be traced to polycritical states (see, for example, Refs. 11–13). Without any additional parameters but using the empirical turbulent mean profile as basic flow input, Jang *et al.*[14] found a bicritical direct resonance between three-dimensional (3-D) primary Orr–Sommerfeld and vertical vorticity (Squire) modes. They used this to explain the preferred scales of 3-D disturbances in turbulent flow.

For the classical Blasius boundary layer, and its parallel-flow paradigm plane Poiseuille flow, it is well known (cf. Herbert[15]) that the two-dimensional (2-D) finite-amplitude primary instability waves become unstable to 3-D *secondary* instabilities, but the consecutive bifurcations and their importance for the transition process are still poorly understood. Using 2-D equilibrium solutions in a Blasius boundary layer[16,17] as base flow it was shown by Koch,[16] that two neutral phase-locked temporal secondary instability modes can coincide to form a bicritical, nonsemisimple resonance. Here nonsemisimple means that only one eigenfunction exists for the two coinciding eigenvalues. Equilibrium solutions are very special, generally unstable solutions of the Navier–Stokes equations possibly related to the large-scale

 1070-6631/95/7(6)/1282/10/$6.00

coherent structures observed in transitional or turbulent flow (cf. Saffman,[18] Newell *et al.*[19]). But they have the advantage that, aside from the parallel-flow assumption used in our investigation, no modeling or empirical input is needed.

In the present work, we investigate the nonlinear solution in the vicinity of this bicritical modal degeneracy in the hope of finding some clues for the transition mechanism. Similar to our previous local analysis near semisimple degenerate bifurcation points in plane Poiseuille flow,[20] the relevant nonlinear normal form equations are derived by a numerical reduction on the center manifold.[10] In the present Blasius boundary-layer case this leads to the symmetrical Takens–Bogdanov normal form. Of prime interest is the appearance of a homoclinic bifurcation which possibly is the dynamical origin of a bursting process. To test the local predictions we also performed a global numerical continuation analysis for equilibrated 3-D waves in the full Navier–Stokes system. While the predicted tertiary Hopf bifurcations were verified for the full system, the homoclinic bifurcations can only be detected by a dynamical full scale simulation which is outside the scope of the present investigation.

II. FORMULATION OF THE PROBLEM AND LINEAR RESULTS

We consider the flow of an incompressible viscous fluid of constant kinematical viscosity ν^* past a semi-infinite flat plate located at $y^*=0$, $0\leqslant x^*$, $-\infty<z^*<\infty$. In order to compute the basic (laminar) state for this geometry, we impose certain simplifying assumptions, most stringent of all the parallel-flow assumption.[16] By introducing an artificial force term, the laminar Blasius boundary layer becomes an exact solution of the Navier–Stokes equations. This is a weak point of our approach, but as shown by Bertolotti and Herbert[21] the effect of nonparallelity is small as long as the direction of wave propagation does not deviate too much from the mean-flow direction. With increasing deviations from the basic Blasius flow, this force term is kept constant in our formulation. This corresponds to a *constant wall shear stress*, analogous to the constant pressure gradient formulation for plane Poiseuille flow.[22] Similar to the changed center-line velocity in plane Poiseuille flow, the free-stream velocity far from the plate will therefore also differ from the laminar free stream velocity U_∞^*. The use of the physically more realistic *constant free stream velocity* boundary condition necessitates the use of a variable force term.[17,23]

Introducing the self-similarity reference length $L^* = (\nu^* x^*/U_\infty^*)^{1/2}$, the quasiparallel Blasius profile depends only on the nondimensional coordinate $y=y^*/L^*$ normal to the wall. Superimposing a disturbance velocity $\mathbf{v}=(u,v,w)$ and pressure perturbation p to the quasiparallel Blasius boundary-layer flow $[U(y),0,0]$, the Navier–Stokes equations can be written in the primitive variable formulation

$$\frac{\partial \mathbf{v}}{\partial t}+[U(y)-C]\frac{\partial \mathbf{v}}{\partial x}+v\frac{dU}{dy}(y)\mathbf{i}+\nabla p-\frac{1}{\mathrm{Re}}\Delta \mathbf{v} +(\mathbf{v}\cdot\nabla)\mathbf{v}=0, \tag{1}$$

Here $\mathrm{Re} = U_\infty^* L^*/\nu^* = (U_\infty^* x^*/\nu^*)^{1/2}$ is the local Reynolds number and $\mathbf{i}$ denotes the unit vector in the nondimensional streamwise direction $x=x^*/L^*$. The equations have been transformed to a frame of reference moving with the (unknown) wave speed C in the streamwise direction, where initially C is determined by the 2-D traveling-wave equilibrium solution. In this moving frame of reference the flow is steady, i.e., $\partial/\partial t\equiv 0$. Equations (1) are subject to the no-slip condition for $\mathbf{v}$ at the wall $y=0$ and to appropriate decay conditions at infinity for all fluctuating quantities. Only the mean-flow correction remains finite and satisfies a Neumann boundary condition at infinity due to the constant wall shear stress condition.[16]

The system (1) can be reformulated in terms of the normal velocity v and the normal vorticity $\eta=\partial u/\partial z-\partial w/\partial x$ as independent variables.[22,24] The solution is assumed to be periodic in the streamwise x direction, as well as spanwise z direction with wavelengths $\lambda_x=2\pi/\alpha$ and $\lambda_z=2\pi/\beta$, respectively. Then the independent flow quantities can be expressed as (truncated) modal expansions

$$\begin{Bmatrix} v(x,y,z,t) \\ \eta(x,y,z,t) \end{Bmatrix} = \sum_{n=-N}^{N}\sum_{m=-M}^{M} \begin{Bmatrix} \hat{v}_{nm}(y,t) \\ \hat{\eta}_{nm}(y,t) \end{Bmatrix} \times \exp[i(n\alpha x+m\beta z)]. \tag{2}$$

According to Squire's theorem, the critical Reynolds number is reached via 2-D linear Tollmien–Schlichting waves. Starting with these on the neutral curve, a numerical continuation procedure provides the *nonlinear 2-D equilibrium surface* ($M=0$), as described in Ref. 16, where the surface of the nonlinear Tollmien–Schlichting waves was computed for various Fourier truncations N. Besides the description of the 2-D neutral surface, Ref. 16 also contains a secondary stability analysis of these nonlinear solutions. The basic state (the 2-D nonlinear equilibrium solution) is periodic in the streamwise direction x and its stability, with respect to three-dimensional disturbances, can be computed by applying Floquet theory.[15] Concentrating on fundamental parametric resonances, corresponding to phase-locked disturbances of Klebanoff-type (cf. Ref. 15), the existence of a bicritical direct resonance, that is a nonsemisimple resonance, was detected in Ref. 16. Interestingly, this modal degeneracy occurs for a Reynolds number in the range of the experimentally observed transition Reynolds number for Blasius flow (cf. Fig. 10 in Ref. 16).

The analysis of this modal degeneracy between three-dimensional secondary instability modes is the main topic of this paper. Using a streamwise truncation $N=2$ and $K=30$ Chebyshev polynomials in the wall normal direction, the resonance occurs on the 2-D equilibrium surface for $\mathrm{Re}=882$ and $\alpha=0.232\,891\,3$. The upper part of Fig. 1 shows the corresponding cuts through the 2-D neutral surface in the (E,α) and (E,Re) plane, respectively, E being the 2-D fluctuation energy.[16] The bicritical point (marked by the open circle in Fig. 1) is located below the turning point of the 2-D equilibrium solution, where instabilities due to (superharmonic) 2-D disturbances are also expected. Hence, before investigating the resonance between 3-D instability modes, we briefly discuss 2-D instability. Two-dimensional *secondary instability* can be computed via Floquet analysis (see, for example,

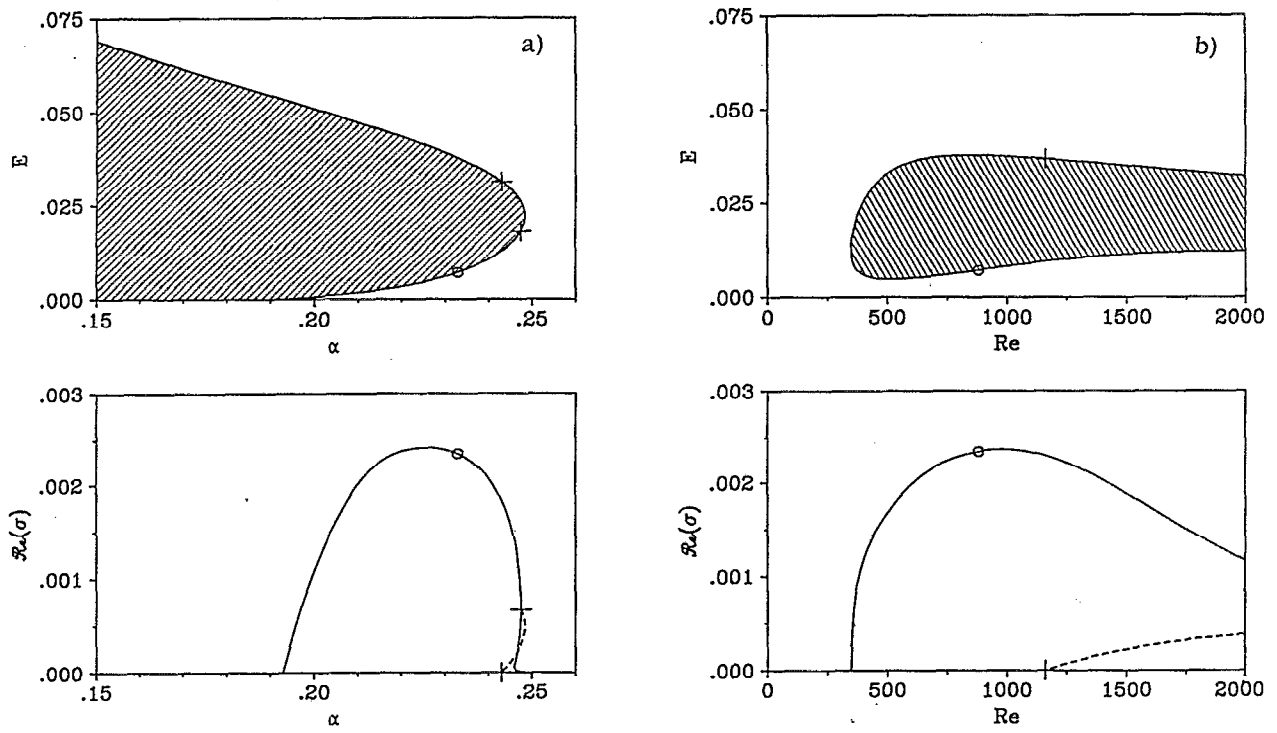

FIG. 1. Amplification rate $\mathrm{Re}(\sigma)$ of superharmonic 2-D phase-locked (solid lines in lower figures) and nonphase-locked (dashed lines) secondary instability modes as function of streamwise wave number α for Re=882 (a), or as function of Reynolds number Re for α=0.232 891 3 (b) with N=2. The upper part of the figures shows the corresponding cuts through the 2-D neutral surface, E being the 2-D fluctuation energy. The location of the bicritical point is marked by open circles.

Pugh and Saffman[25] or Soibelman and Meiron[26] for the corresponding plane Poiseuille flow case). In our moving frame of reference the 2-D equilibrium solution is steady, so that we may obtain its stability, with respect to 2-D superharmonic disturbances, as a byproduct of the 2-D continuation procedure. Linearizing the time-dependent equations around the 2-D equilibrium solution, we may use the Jacobian of the continuation procedure to formulate a large generalized eigenvalue problem. To minimize numerical errors this generalized eigenvalue problem is reduced to an ordinary eigenvalue problem which is then solved by a standard eigenvalue routine.

After eliminating the phase-shift eigenvalue σ=0, a consequence of the translational invariance in streamwise direction (cf. Pugh and Saffman[25]), the 2-D equilibrium solution is unstable to 2-D secondary disturbances if the real part of the largest eigenvalue $\max_\sigma \mathfrak{Re}(\sigma)>0$. For the Re=const and α=const cuts through the bicritical point (marked by the circle) the resulting amplification rates $\mathfrak{Re}(\sigma)$ are shown in the lower part of Fig. 1. Phase-locked 2-D instability modes [$\mathfrak{Re}(\sigma)>0$, $\mathfrak{Im}(\sigma)=0$, depicted by solid lines] are observed on the lower branch, while nonphase-locked instability modes [$\mathfrak{Re}(\sigma)>0$, $\mathfrak{Im}(\sigma)\neq 0$, depicted by dashed lines] appear near the turning point, as well as for higher Reynolds numbers on the upper branch (compare the corresponding plane Poiseuille flow results[25–27]). The amplification rate at the bicritical point is again marked by a circle.

The secondary amplification rates $\mathfrak{Re}(\sigma)$ for *3-D secondary disturbances* are depicted in Fig. 2 as functions of the spanwise wave number β for Re=882 and α=0.232 891 3. The solid lines in Fig. 2 represent phase-locked modes (i.e., these modes generate 3-D solutions traveling with the phase speed of the 2-D solution), dashed lines show nonphase-locked modes corresponding to quasiperiodic solutions in the laboratory frame of reference. One observes the *modal de-*

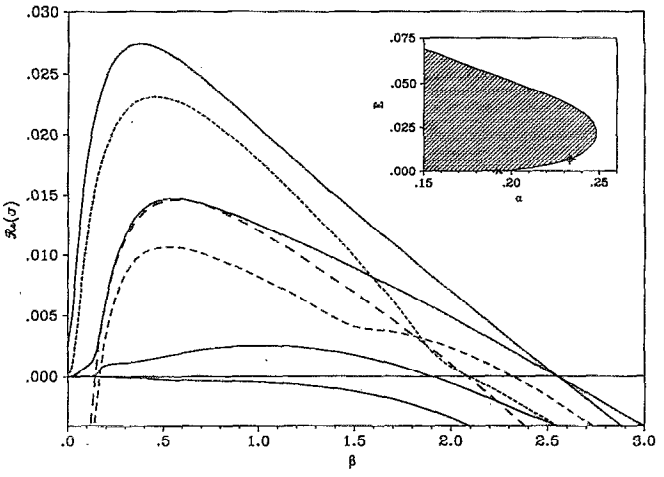

FIG. 2. Amplification rate $\mathrm{Re}(\sigma)$ of 3-D phase-locked (solid lines) and nonphase-locked (dashed lines) secondary instability modes as function of spanwise wave number β on the 2-D equilibrium surface for Re=882, α=0.232 891 3, N=2. The point in the insert marks the position of the modal coincidence (at β=2.554) on the 2-D neutral surface.

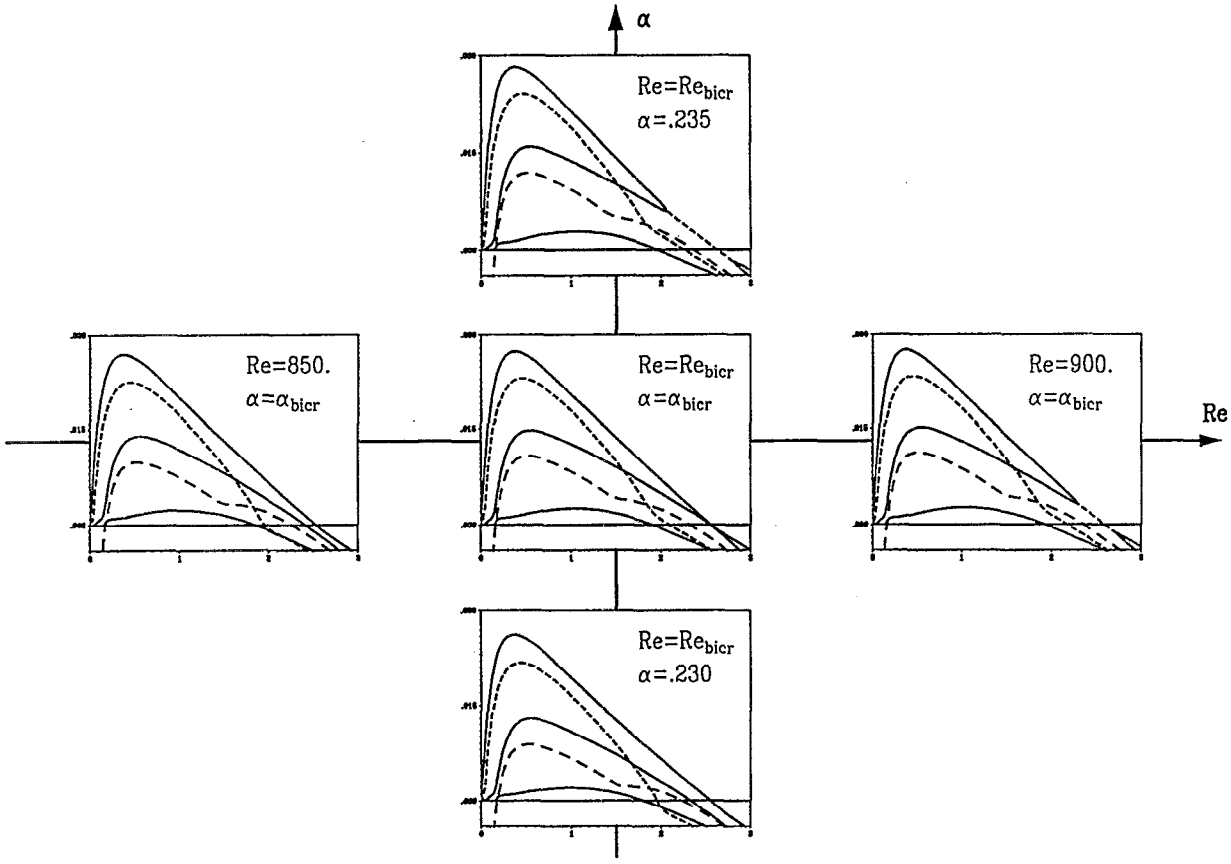

FIG. 3. Change of phase-locked (—) and nonphase-locked (---) 3-D secondary amplification rates as function of spanwise wave number β in the vicinity of the $N=2$ bicritical bifurcation point at $(\alpha_{bicr}, Re_{bicr})=(0.232\ 891\ 3,\ 882)$.

generacy between the first and second phase-locked mode at $\beta=2.554$. Only minor deviations are observed from the bicritical $N=3$ result of Ref. 16, such that one can be fairly confident that nonlinear dynamics of our truncated system (at $N=2$) is in qualitative agreement with the full solution near the degeneracy. Again, the insert of Fig. 2 shows the position of the resonance on the 2-D neutral surface (for Re=882) in the (E, α) plane. We note that the maximal amplification rate of the 3-D disturbances is an order of magnitude higher than that of the 2-D disturbances (cf. Fig. 1) clearly indicating the dominance of 3-D secondary instabilities (cf. Herbert[15]).

The occurrence of a bicritical resonance between 3-D secondary instability modes is possibly of importance for the transition process. This modal degeneracy implies the existence of a double zero eigenvalue with only one eigenvector, indicating a nonsemisimple resonance (cf. Ref. 28) leading to an algebraic growth of secondary amplitudes.[16] For instance, the secondary temporal growth at the bicritical point $\beta_{bicr}=2.554$ is proportional to t (see next section). For a certain transient time this algebraic growth is the dominant one, because the amplification rates of nearby exponentially amplified modes (i.e., for $\beta<\beta_{bicr}$ in Fig. 2) are small. Also, the existence of this resonance provides a rare opportunity to apply bifurcation theory to finite-amplitude solutions of the Navier–Stokes equations. Figure 3 summarizes the linear connect-and-cut process between the phase-locked secondary modes in the vicinity of the bicritical bifurcation point (α_{bicr}, Re_{bicr}). Of particular interest is that a local (positive) change in the parameter values leads to the appearance of a Hopf bifurcation. This obviously results from the mode interaction. We note that in 2-D plane Poiseuille flow similar secondary Hopf bifurcations have been predicted as a result of a resonance between secondary 2-D modes.[29] Those secondary Hopf bifurcations also lead to quasiperiodic solutions, since the basic state is a traveling wave.[26,27,29] Computations of those 2-D solutions for plane Poiseuille flow can be found in Ref. 26. In our Blasius flow computation, the resonance occurs between 3-D disturbances. It is generally believed that three-dimensionality is essential for the transition process. We therefore disregard the weak instabilities resulting from 2-D secondary disturbances, and concentrate on the resonance of the 3-D secondary instability modes whose amplification rates are typically an order of magnitude higher. For the corresponding local reduction to be significant it is important to note that for the β value of resonance all other 3-D secondary stability modes are damped (cf. Fig. 2).

III. LOCAL NONLINEAR REDUCTION

The nonsemisimple resonance is a bifurcation point of algebraic multiplicity two and geometric multiplicity one. Therefore, the description of the local behavior necessitates the computation of the generalized nullspace of the 3-D Jacobian $\mathbb{J}\equiv\mathbb{J}$ ($\mathbf{v}_{2D}$, α_{bicr}, Re_{bicr}, β_{bicr}) at the degenerate bi-

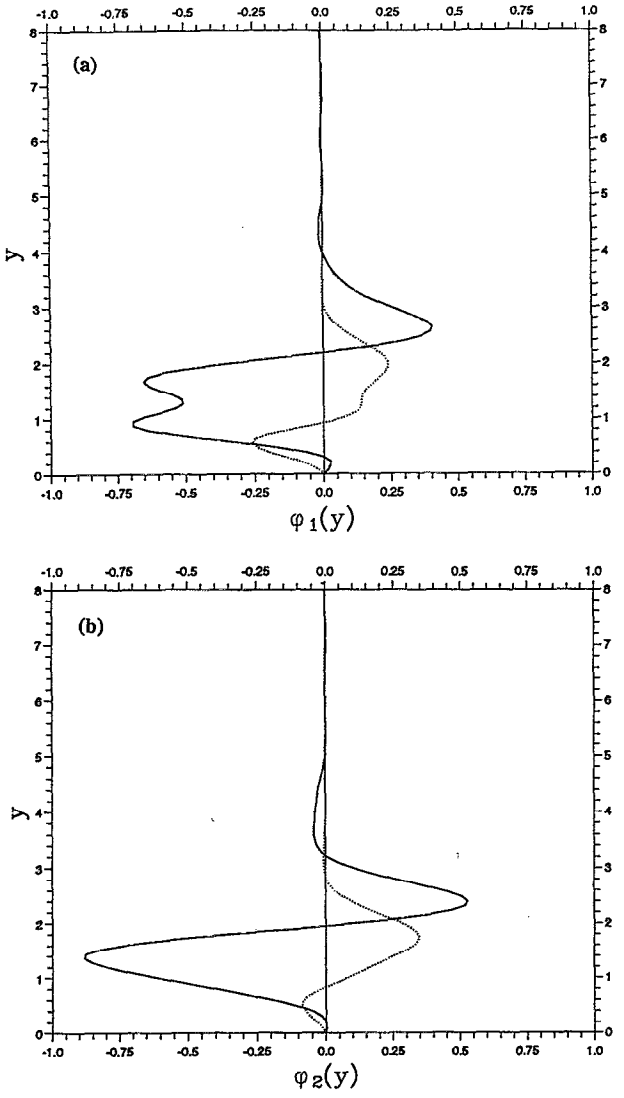

FIG. 4. Real part (—) and imaginary part (···) of the $\hat{\eta}_{11}(y)$ component of the secondary neutral eigensolution (a), as well as of the generalized secondary eigensolution (b) in the bicritical bifurcation point at Re=882, α=0.232 891 3, β=2.554.

furcation point (cf. Ref. 28). The computation of the 3-D Jacobian can be performed by extending our 3-D continuation analysis[22] to quasiparallel boundary-layer flow. Using the constant force term formulation, preliminary 3-D equilibrium results for spanwise symmetric oblique waves in a quasiparallel Blasius boundary layer are reported in Ref. 24.

The 3-D secondary eigensolutions φ are single β modes of the general form

$$\begin{Bmatrix} v(x,y,z) \\ \eta(x,y,z) \end{Bmatrix} = \exp(i\beta z) \sum_{n=-N}^{N} \begin{Bmatrix} \hat{v}_{n1}(y) \\ \hat{\eta}_{n1}(y) \end{Bmatrix} \exp(in\alpha x).$$

Figures 4(a) and 4(b) show a component of the secondary eigenfunction φ_1, as well as of the generalized eigenfunction φ_2, which is a solution of the system

$$\mathbb{J}\varphi_2 = \gamma\varphi_1$$

for an appropriate constant of normalization γ. The *center manifold reduction* provides a powerful technique in order to describe the local bifurcation behavior.[10,30] If we denote the generalized nullspace by E^c, the center manifold theorem stipulates the existence of a center manifold W^c tangent to E^c at the bifurcation point. The reduced system is then obtained by projection onto E^c. If there is no unstable eigenspace E^u at the bifurcation point, the reduced system determines the stability of the global system.[30] In our case, the physically most important instabilities are 3-D and, as noted before, E^u is empty for the family of 3-D disturbances in the degenerate bifurcation point.

Similar to our plane Poiseuille flow study,[20,22] we assume that the bifurcating 3-D solutions are invariant with respect to the spanwise reflection $z \to -z$. Accordingly, the continuous translation in the spanwise direction $z \to z+l$ reduces to the discrete one $z \to z+\lambda_z/2$, λ_z being the wavelength in the z direction. Since the secondary modes generating the generalized nullspace are single β modes, this leads to a symmetry operator S such that

$$S\varphi_1 = -\varphi_1, \quad S\varphi_2 = -\varphi_2.$$

We denote by x_i, $i=1,2$, the (local) amplitudes of φ_i, $i=1,2$. Then the representation of S in the amplitude space is given by

$$(x_1, x_2) \to (-x_1, -x_2).$$

The reduced system is equivariant with respect to this symmetry and its Taylor expansion containing all cubic terms in the amplitude variables is

$$\begin{aligned} \dot{x}_1 &= x_2 + \delta_{11}x_1 + \delta_{12}x_2 + a_1x_1^3 + a_2x_1^2x_2 + a_3x_1x_2^2 + a_4x_2^3, \\ \dot{x}_2 &= \delta_{21}x_1 + \delta_{22}x_2 + b_1x_1^3 + b_2x_1^2x_2 + b_3x_1x_2^2 + b_4x_2^3, \end{aligned} \tag{3}$$

where the δ_{ij} are functions of the local changes in the physical parameters α, β, and Re.

The various coefficients of (3) were computed by numerical projection of the global, discrete system (truncated at $N=M=2$) onto the center manifold and are listed in the Appendix [we have used ln(Re) instead of Re in order to normalize the corresponding coefficients]. In our computation we kept only the linear dependence of δ_{ij} on the parameter changes $\delta\alpha$, $\delta\beta$ and δ[ln(Re)], which is sufficient for a qualitative, local analysis. The corresponding algorithm is tedious but straightforward. The different terms of the Taylor expansion of the center manifold are obtained by solving a sequence of linear systems together with the so-called Fredholm alternative.[31] For $\delta_{ij}=0$ in (3) (that is at the bicritical point), linearization leads to the linear algebraic growth in t for x_1, which corresponds to the transient growth of the secondary eigensolution, mentioned in Sec. II.

In the following, we try to check the correspondence between the stability of the trivial solution of (3) and the numerically obtained linear secondary stability results depicted in Fig. 3. Introducing a small amplitude ϵ and performing the following scaling in amplitude variables, parameters and time

$$x_1 = \epsilon\xi_1, \quad x_2 = \epsilon^2\xi_2, \quad \delta_{ij} = \epsilon^2\bar{\delta}_{ij}, \quad \tau = \epsilon t,$$

to emphasize the differing order of magnitude, Eq. (3) becomes up to first order in ϵ

$$\dot{\xi}_1=\xi_2+\epsilon\bar{\delta}_{11}\xi_1+\epsilon a_1\xi_1^3$$

$$\dot{\xi}_2=\bar{\delta}_{21}\xi_1+\epsilon\bar{\delta}_{22}\xi_2+b_1\xi_1^3+\epsilon b_2\xi_1^2\xi_2.$$

The stability of the trivial solution (which corresponds to the 2-D equilibrium state) is then given by the eigenvalues of the Jacobian

$$\begin{pmatrix}\epsilon\bar{\delta}_{11} & 1\\ \bar{\delta}_{21} & \epsilon\bar{\delta}_{22}\end{pmatrix}.$$

Steady bifurcations occur for parameter values such that

$$\delta=\epsilon^2\bar{\delta}_{11}\bar{\delta}_{22}-\bar{\delta}_{21}=0, \tag{4}$$

whereas Hopf bifurcations occur for

$$\bar{\delta}_{11}+\bar{\delta}_{22}=0, \quad \delta>0, \tag{5}$$

with δ defined by (4). Keeping for instance the Reynolds number fixed at its bicritical value and introducing the scaled wave-number deviations $\delta\alpha=\epsilon^2\bar{\delta}\alpha$ and $\delta\beta=\epsilon^2\bar{\delta}\beta$, we obtain

$$\epsilon^2 55.77\,\bar{\delta}\beta^2+(0.04-\epsilon^2 4103.04\,\bar{\delta}\alpha)\,\bar{\delta}\beta$$

$$+\epsilon^2 16\,336.28\,\bar{\delta}\alpha^2+154.49\,\bar{\delta}\alpha=0, \tag{6}$$

by substituting into Eq. (4) the values given in the Appendix.

Figure 3 depicts results for $|\delta\alpha|<0.003$. Therefore, an appropriate scaling would be $\epsilon=0.05$, and (6) becomes approximately

$$0.14\,\bar{\delta}\beta^2+(0.04-10.26\,\bar{\delta}\alpha)\,\bar{\delta}\beta+40.84\,\bar{\delta}\alpha^2$$

$$+154.49\,\bar{\delta}\alpha=0. \tag{7}$$

For $\bar{\delta}\alpha<0$ (of the order of one) in (7) there will be two roots for $\bar{\delta}\beta$ indicating two steady bifurcation points. They correspond to the phase-locked bifurcation points of Fig. 3 for $\delta\alpha<0$. For $\bar{\delta}\alpha>0.000\,02$, Eq. (7) has no real roots (with $\bar{\delta}\alpha$ of order one). This lower bound is outside the accuracy of our computation, because it corresponds to a real deviation of $\delta\alpha=10^{-8}$ (and α_{bicr} has only been computed up to seven digits). Therefore, there are locally no steady-state bifurcations for $\delta\alpha>0$.

To see whether the Hopf bifurcations are predicted correctly, we substitute the numerical values listed in the Appendix into (5) and obtain $\bar{\delta}\beta=34.95\,\bar{\delta}\alpha$. The left-hand side of (7) will be positive for values of $\bar{\delta}\alpha$ bounded by one. In terms of the real deviation, $\delta\alpha$, this would correspond to a value of about 0.0025. The conditions (5) for a Hopf bifurcation to occur are satisfied, which again is in agreement with Fig. 3. In order to get further information about the validity of relation (7), we put $\bar{\delta}\alpha=0$ in (7): there are two zeros, $\bar{\delta}\beta=0$ and $\bar{\delta}\beta\approx-0.29$. The second value is obviously spurious, because for $\bar{\delta}\alpha=0$ and fixed Reynolds number there is locally only the bicritical bifurcation point for $\bar{\delta}\beta=0$. In terms of the real deviation, the above value corresponds approximately to $\delta\beta\approx-0.0007$. However, we only determined the bicritical β value ($\beta_{\text{bicr}}=2.554$) up to about three digits, hence the spurious $\delta\beta$ value is outside the accuracy of our computation. Similarly, for $\bar{\delta}\beta=0$ we find the two roots $\bar{\delta}\alpha=0$ and $\bar{\delta}\alpha\approx-3.78$, the second value corresponding to the streamwise wave-number deviation $\delta\alpha\approx-0.01$. This value is again outside the validity of our local analysis because already very small deviations from $\alpha_{\text{bicr}}=0.232\,891\,3$ ($|\delta\alpha|<0.003$ in Fig. 3) lead to significant changes in the secondary linear stability behavior. This is the reason why we had to compute α_{bicr} up to seven digits. A similar analysis could be performed by keeping α_{bicr} fixed, while varying the Reynolds number in the vicinity of $\text{Re}_{\text{bicr}}=882$.

The above scaling has been introduced in order to quantitatively relate the numerically computed linear secondary stability results to the stability of the trivial fixed point of the center manifold equations (3). In Sec. IV we shall attempt a quantitative comparison with our global nonlinear computation. However, at the center of our interest is the qualitative dynamical behavior in the vicinity of the bicritical point on the 2-D equilibrium surface. For that purpose the *normal form technique* provides a powerful tool to transform (3) into a simpler form.[10] This can be achieved by a (nonlinear) coordinate transformation which preserves the degree of approximation of the vector field on the center manifold. The simplified system exhibits then the same qualitative dynamics as the original one. For our example, the coordinate change

$$x_1=y_1+\tfrac{1}{3}\,(\tfrac{1}{2}b_3+a_2)y_1^3+\tfrac{1}{2}(b_4+a_3)y_1^2y_2+a_4y_1y_2^2,$$

$$x_2=y_2+\tfrac{1}{2}b_3y_1^2y_2+b_4y_1y_2^2-a_1y_1^3-\delta_{11}y_1-\delta_{12}y_2 \tag{8}$$

leads to the following normal form containing all cubic terms in the transformed amplitude variables:

$$\dot{y}_1=y_2,$$

$$\dot{y}_2=\mu_1y_1+\mu_2y_2+ay_1^3+by_1^2y_2, \tag{9}$$

where $\mu_1=\delta_{21}$, $\mu_2=\delta_{11}+\delta_{22}$, $a=b_1$, $b=b_2+3a_1$.

The normal form (9) is of the *symmetrical Takens–Bogdanov type*[10] and the local bifurcation behavior can be described as function of the two bifurcation parameters μ_1 and μ_2. With the numerical values listed in the Appendix the coefficients in the normal form (9) are

$$a=-0.21, \quad b=19.01. \tag{10}$$

Their respective sign is important to determine the type of local dynamics that occurs.

The bifurcation behavior for normal forms similar to the system (9) has been discussed for example in the context of double-diffusive systems.[32] For the unfolding of (9) we follow the treatment given in Ref. 10. The (local) stability of the trivial solution $(y_1,y_2)=(0,0)$ (which, in our case, corresponds to the 2-D nonlinear traveling wave) is given by the real part of the eigenvalues of the linearized system

$$\mu_2/2\pm\sqrt{(\mu_2/2)^2+\mu_1}. \tag{11}$$

Consequently, the trivial fixed point undergoes a Hopf bifurcation for

$$\mu_2=0, \quad \mu_1<0, \tag{12}$$

which corresponds qualitatively to the Hopf bifurcation for the fixed point of (3). The (local) stability of the Hopf bifurcation can be determined through normal form computations.[10] In our case, the coefficient b in the normal

form (9) is positive [cf. (10)], therefore the bifurcation is subcritical and there is locally an unstable family of periodic orbits surrounding the sink for $\mu_1,\mu_2<0$.

The nontrivial fixed points for the normal form (9) are given by

$$y_1^2=-\mu_1/a, \quad y_2=0. \tag{13}$$

They bifurcate as pitchforks for $\mu_1>0$, the coefficient a being negative [cf. (10)]. Linearizing at these points, their stability is determined by the real parts of

$$\mu/2\pm\sqrt{(\mu/2)^2-2\mu_1}$$

with

$$\mu=\mu_2-b\mu_1/a. \tag{14}$$

Consequently, the pair of fixed points (13) undergoes a Hopf bifurcation for

$$\mu=0, \quad \mu_1>0. \tag{15}$$

The nontrivial fixed points (13) correspond qualitatively to steady-state bifurcations of (3) and hence locally to 3-D traveling waves for the global Blasius flow problem. Consequently, the Hopf bifurcations (15) can be interpreted as *tertiary bifurcations* to quasiperiodic solutions. Using again normal form computations it can be shown that these Hopf bifurcations are supercritical leading to locally stable periodic orbits surrounding the pair of sources (13) for $\mu_2>b\mu_1/a$. For the normal form there is only one pitchfork bifurcation as function of μ_1. However, μ_1 depends on the three physical parameters and an accurate nonlinear expansion of μ_i, $i=1,2$, in terms of the physical parameters is needed to obtain quantitative results [for instance, two separate bifurcation points would appear in the physical parameter space, as demonstrated in the discussion of system (3) in Sec. IV]. Also the *physical* amplitudes (x_1,x_2) depend on the normal form amplitudes by inclusion of the parameters via δ_{11} and δ_{12} in (8), which is a further difficulty in an actual quantitative comparison.

Normal forms of the type (9) are known to undergo a (double) saddle connection for particular values of the parameters.[10] Using a scaling analysis it can be shown (cf. Ref. 10) that the homoclinic bifurcation occurs approximately on the line

$$\mu_2=4b\mu_1/(5a), \quad \mu_1>0. \tag{16}$$

The bifurcation behavior of the system (9) is summarized in Fig. 5. For each major region in the (μ_1,μ_2) plane we computed the corresponding phase portrait. For $\mu_1>0$ the lines *bh* and *bsc* correspond to the location of the Hopf bifurcation and the homoclinic bifurcation given by (15) and (16), respectively [note that the actual slope of these lines, given by b/a and $4b/(5a)$, respectively, is not drawn to scale]. For clarity, the phase portraits have been computed for normalized coefficients $a=-1$ and $b=1$ in the normal form (9). This ensures a qualitatively correct picture, since these coefficients have the same sign as the actual ones given by (10). Note that the homoclinic orbit on the line *bsc* in the parameter space is stable for our normal form.

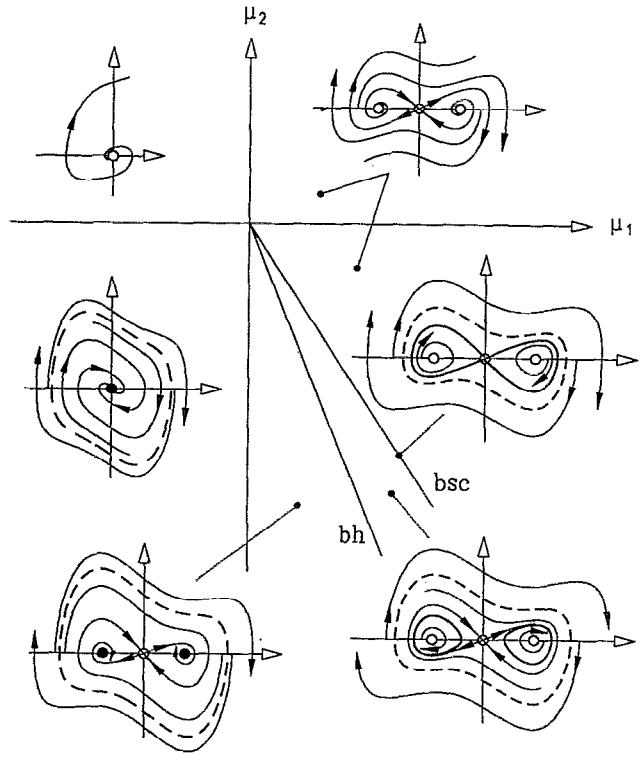

FIG. 5. Bifurcation diagram of normal form (9) with a sketch of the associated phase portraits. Line *bh*: location of the Hopf bifurcation. Line *bsc*: location of the double saddle connection (homoclinic bifurcation).

IV. GLOBAL BIFURCATION ANALYSIS

To check some predictions of the local theory we performed a continuation analysis in the (α, β, Re) parameter space for 3-D phase-locked waves of the full Navier–Stokes equations. For this purpose we used highly truncated solutions (2) with $N=M=2$. Applying Keller's[33] pseudo-arclength continuation procedure we extended our spanwise symmetric plane Poiseuille flow analysis[22] to Blasius boundary layer flow as outlined in Ref. 24. Due to the spanwise symmetry only modes in the first quadrant have to be retained. In contrast to Ref. 24, where a symmetric pair of neutral primary oblique waves was the starting point of the continuation process, we start now with the neutrally stable secondary phase-locked waves on the 2-D nonlinear equilibrium surface $N=2$, $M=0$.

First, we keep Re=882 const and choose $\alpha=0.2328$ slightly below the bicritical $\alpha=0.232\,891\,3$. According to the linear results of Fig. 3, two phase-locked secondary bifurcation branches emanate near the bicritical $\beta=2.554$ on the lower 2-D branch $E_{2D}^{(l)}=0.007\,029$. The continuation result is depicted in the enlarged insert of Fig. 6, with the inverted triangles marking the secondary pitchfork bifurcation points predicted by the linear secondary stability analysis, as well as by the local system on the center manifold (3). For the particular example chosen, the 3-D branch simply connects the two phase-locked bifurcation points and has no connection to the upper 2-D branch at $E_{2D}^{(u)}=0.037\,69$. Again, using the Jacobian of the continuation procedure, a 3-D superharmonic stability analysis shows that shortly after sec-

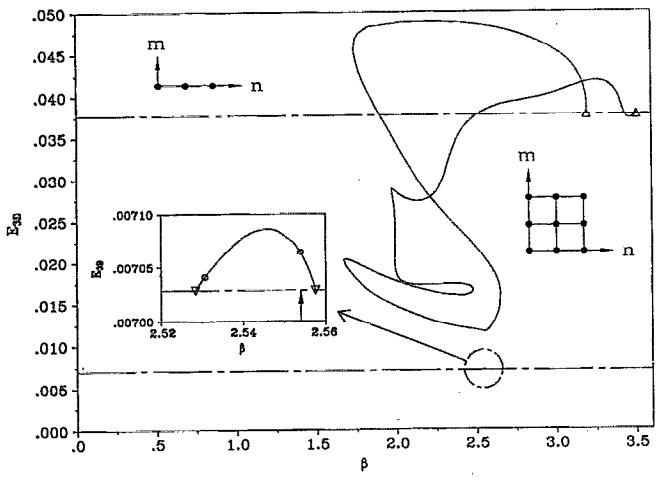

FIG. 6. Re=882, α=0.2328 cut through the 3-D equilibrium surface with $N=M=2$. Enlarged insert shows the 3-D branch in the vicinity of the bicritical bifurcation point β=2.554 (marked by the arrow) on the lower 2-D branch. The location of the tertiary Hopf bifurcations is marked by the open circles.

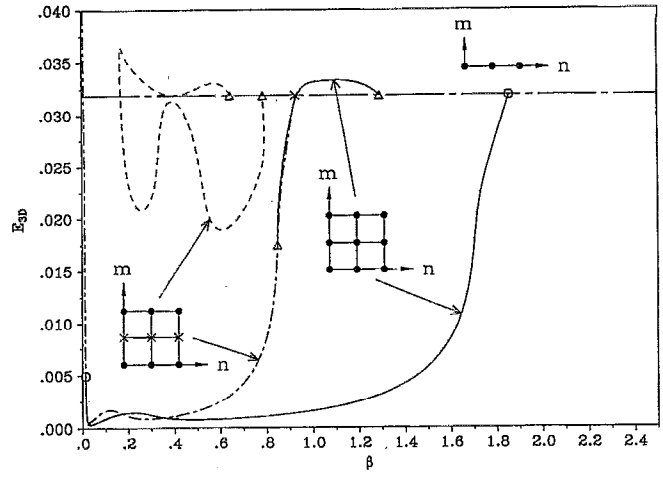

FIG. 7. Re=350, α=0.2 cuts through the 3-D equilibrium surface, with $N=M=2$. 3-D bifurcating branches with all Fourier modes excited (—), or with only even spanwise harmonics excited (----;---).

ondary bifurcation a Hopf bifurcation (marked by the open circles) occurs in the moving frame in addition to the 2-D phase-locked instability.

Our local bifurcation analysis of Sec. III is mainly concerned with qualitative results about the dynamics in the vicinity of the 2-D equilibrium solution. Following a referee's suggestion, we attempt to quantitatively relate our global results of Fig. 6 to the local center manifold system (3). Phase-locked bifurcations on the 2-D equilibrium state correspond to steady-state bifurcation points of (3), hence they are given by (4). The global results depicted in the insert of Fig. 6 have been computed for the bicritical Reynolds number Re=882, and a change in the streamwise wave number with respect to the bicritical value of $\delta\alpha=-0.000\,091\,3$. With the scaling $\epsilon^2=0.0025$ (cf. Sec. III) this corresponds to $\bar{\delta}\alpha=-0.0365$ in (7). Substituting this value, (7) becomes approximately

$$0.14\bar{\delta}\beta^2+0.41\bar{\delta}\beta-5.58=0,$$

the zeros being the scaled spanwise wave-number deviations $\bar{\delta}\beta=5.02$ and $\bar{\delta}\beta=-7.95$. Multiplying by $\epsilon^2=0.0025$ one gets $\delta\beta\approx 0.0126$ and $\delta\beta\approx -0.0199$. These quantities should correspond to the deviation of the β values of the secondary bifurcation points from the bicritical $\beta_{\text{bicr}}=2.554$ marked by the vertical arrow in the insert of Fig. 6. A comparison with the results of the global computation (the numerically obtained bifurcation points are marked by upside down triangles in the insert of Fig. 6) shows that these values only approximate the deviations. To obtain more accurate results would necessitate a Taylor expansion of (3) to higher orders in the parameter values (and perhaps a more accurate determination of β_{bicr} and Re_{bicr}) which would be a tedious task. A separate analysis of the two bifurcating steady-state branches of Eq. (3), with the approximate bifurcation points given by the two $\delta\beta$ values computed above, would predict the Hopf bifurcations occurring on the global 3-D branches (cf. insert Fig. 6). The existence of those Hopf bifurcations on the 3-D branches in the vicinity of the 2-D equilibrium state can more easily be predicted by an analysis of the normal form (9). We must emphasize again that system (9) describes the qualitative dynamics in the vicinity of the 2-D state, and that this qualitative description is the main object of our local analysis. The global computation confirms the normal form prediction of nontrivial fixed points which lose their stability by undergoing Hopf bifurcations (cf. Fig. 5). However, our local analysis cannot predict the connection between the two 3-D branches shown in Fig. 6.

Since the bifurcating branches on the lower 2-D branch are not connected to the upper branch, as we originally expected, we started the continuation also at the phase-locked bifurcation points on the 2-D upper branch, marked by upright triangles in Fig. 6. [The corresponding local skin friction factor defined by $c_f' = \tau^*_{\text{wall}}/\frac{1}{2}\rho^* u^*_m(\infty)^2$ is shown as line 2 in Fig. 8. Here τ^*_{wall} is the dimensional wall shear stress, ρ^* the density and $u^*_m(\infty)$ the laminar free-stream velocity at $y=\infty$ reduced by the mean-flow correction. We see that the skin friction factor reaches values near the turbulent experimental results.]

In our present calculation, all modes $|n|\leq 2$, $|m|\leq 2$ are excited as indicated by the dots in the modal pattern of Fig. 6. In Ref. 24 the oblique wave results, computed with the same truncation but giving a chess board like modal pattern for the excited modes, did not give such high friction factors. This encouraged us to search for 3-D equilibrium solutions at lower Reynolds numbers. We chose Re=350 and α=0.2. For these values the linear 2-D solution is unstable and only the upper branch $E^{(u)}_{2D} = 0.031\,84$ exists, cf. Fig. 7. The solid curves bifurcate at the neutral points of the first and the third phase-locked secondary instability modes and end on the dashed–dotted curve as marked by the triangle and open circle. The dashed–dotted curve starts as a spanwise superharmonic of the first phase-locked secondary instability mode. The bifurcation point is marked by a cross and the bifurcating branch only contains even spanwise Fourier modes. In the corresponding modal pattern the excited even

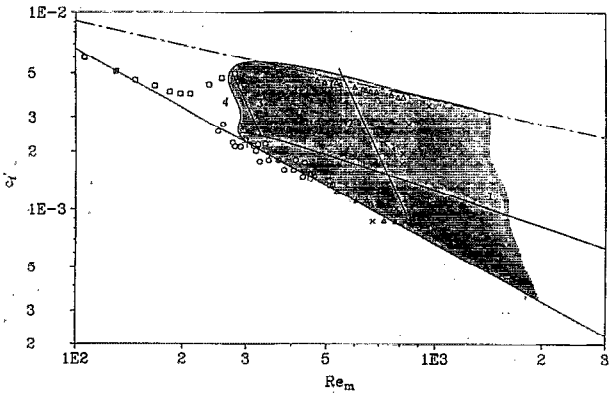

FIG. 8. Local skin friction factor c_f' as a function of modified Reynolds number Re_m. Δ laminar and turbulent skin friction measurements, $\times$ transitional skin friction measurements (Dhawan[35]); o subcritical transition experiment (Asai and Nishioka[36]). (1) Projection of 2-D equilibrium surface, $N=2$. (2) 3-D equilibrium solution, Re=882, $\alpha=0.2328$, $N=M=2$. (3) 3-D equilibrium solution with even spanwise Fourier modes, Re=350, $\alpha=0.2$. (4) 3-D equilibrium solution with even spanwise Fourier modes, $\alpha=0.2$, $\beta=0.4$.

spanwise modes are depicted by dots. The friction factors of these three solution branches do not deviate significantly from the projection of the 2-D neutral surface (curve 1 in Fig. 8). Only when we continued the spanwise superharmonic of the third phase-locked secondary instability mode, depicted by the dashed curve in Fig. 7, did we reach higher c_f' values (line 3 in Fig. 8). We note (cf. Fig. 7) that this branch ends at a bifurcation point corresponding to the spanwise superharmonic of the second phase-locked instability mode, whose branch has not been included here.

Keeping $\alpha=0.2$ and $\beta=0.4$ fixed, we continued the branch, depicted by the dashed curve in Fig. 7, in the Reynolds number Re, extending the 3-D neutral surface to subcritical Reynolds numbers (cf. curve 4 in Fig. 8). The Reynolds number Re_m in Fig. 8 is defined with the actual free-stream velocity $u_m^*(\infty)$ far from the wall, which due to the nonlinear mean-flow correction is lower than the laminar velocity U_∞^*. We note that 3-D equilibrium states containing only even spanwise Fourier modes were also of importance for reaching subcritical Reynolds numbers in plane Poiseuille flow.[22] The domain of our computed equilibrium solutions in the (Re_m, c_f') plane is shown by the shaded area in Fig. 8. Interestingly, these solutions outline almost completely the experimentally found transitional and turbulent data, in contrast to the oblique mode results of Ref. 24.

V. DISCUSSION

Using experimental and numerical simulation, much has been learned about the laminar/turbulent transition process in open flow systems, such as boundary layers. However, the appropriate transition scenario or the exact dynamical mechanism leading to breakdown is still largely unknown. Such an understanding would be the prerequisite for a physically realistic transition criterion which is free of empiricism. One established transition route is via primary and secondary instabilities. But whether tertiary or global bifurcations are the next step is still an open question. Bifurcation theory is one possible tool to shed some light on this. In particular, modal degeneracies are believed to provide useful models for describing a more complex dynamics. At the primary instability level it is well known that for boundary-layer-type flows without additional physical parameters only one single instability mode exists. This primary instability is the starting point for nonlinear states which show a more complex spatial and temporal behavior. These, in general, numerically computed nonlinear solutions are the new basic states for secondary disturbances. Frequently, several secondary instability modes appear allowing for modal degeneracies.

In boundary layers one important class of nonlinear states are 2-D traveling waves. Using 2-D waves which are steady in the moving frame, degeneracies between phase-locked secondary instability modes have been found and provide the basis for our investigation. In terms of dynamical systems theory this degeneracy is a nonsemisimple resonance between two steady, neutral secondary instability modes in the moving frame. The local dynamics can be described by a center manifold reduction.

The corresponding normal form is of the symmetrical Takens–Bogdanov type with numerically computed coefficients. This normal form is of codimension two, the two unfolding parameters μ_1 and μ_2 being implicitly related to the three physical parameters α, β, Re. The phase portraits sketched in Fig. 5 can be interpreted in terms of the qualitative structure and dynamics of the physical problem. Starting at the second quadrant ($\mu_1<0$, $\mu_2>0$) the trivial fixed point at the origin corresponds to the 2-D nonlinear equilibrium wave which is unstable. Proceeding to the third quadrant this fixed point undergoes a subcritical Hopf bifurcation. In the laboratory frame of reference this would correspond to a quasiperiodical solution. Moving into the fourth quadrant two nontrivial stable fixed points appear through pitchfork bifurcations, corresponding to 3-D phase-locked waves. Several of those waves have been computed far beyond the point of degeneracy by means of a global numerical continuation procedure. Crossing the line bh a supercritical Hopf bifurcation occurs on these 3-D branches. They constitute tertiary bifurcations also found in our global computations (cf. Fig. 6). The most interesting dynamical behavior of the normal form occurs on line bsc where the two limit cycles form a locally attracting double-saddle connection. Such homoclinic orbits are often related to intermittent physical bursting or ejection processes, see, for example, Stone and Holmes.[34] Whether this dynamics prevails in the full Navier–Stokes equations can only be checked by a full numerical simulation, which is difficult and far beyond the scope of our present paper.

It is well known that initial and boundary conditions influence transition decisively. Therefore, the 2-D equilibrium solution used as base flow in our analysis provides only very special initial conditions. But we believe that the dynamics found for these special conditions might serve as a model for the more general case. Inclusion of the weak 2-D instability will not change this because 3-D secondary instabilities dominate as demonstrated by numerical simulations. It is also of interest that some of the 3-D equilibrium solu-

tions can be traced to subcritical Reynolds numbers and closely approach the experimental turbulent skin friction data. This would be in line with the hypothesis that equilibria are related to the large-scale coherent flow structures as discussed by Saffman[18] or Newell *et al.*[19]

ACKNOWLEDGMENTS

This work has been supported by travel grants from the French/German program PROCOPE. We are grateful to a referee for helpful suggestions.

APPENDIX: COEFFICIENTS OF TAYLOR EXPANSION (3)

$$\delta_{11}=489.55\,\delta\alpha-7.06\,\delta\beta+22.48\,\delta[\ln(\mathrm{Re})],$$

$$\delta_{12}=11.90\,\delta\alpha+0.40\,\delta\beta-0.93\,\delta[\ln(\mathrm{Re})],$$

$$\delta_{21}=-154.49\,\delta\alpha-0.04\,\delta\beta-4.42\,\delta[\ln(\mathrm{Re})],$$

$$\delta_{22}=33.37\,\delta\alpha-7.90\,\delta\beta+10.83\,\delta[\ln(\mathrm{Re})],$$

$$a_1=0.73,\quad a_2=-61.52,\quad a_3=-722.66,$$

$$a_4=-26.55,$$

$$b_1=-0.21,\quad b_2=16.82,\quad b_3=190.26,$$

$$b_4=-131.51.$$

[1]W. F. Langford, R. Tagg, E. J. Kostelich, H. L. Swinney, and M. Golubitsky, "Primary instabilities and bicriticality in flow between counter-rotating cylinders," Phys. Fluids **31**, 776 (1988).
[2]P. H. Coullet and E. A. Spiegel, "Amplitude equations for systems with competing instabilities," SIAM J. Appl. Math. **43**, 776 (1983).
[3]N. Aubry, P. J. Holmes, J. L. Lumley, and E. Stone, "The dynamics of coherent structures in the wall region of a turbulent boundary layer," J. Fluid Mech. **192**, 115 (1988).
[4]S. Sanghi and N. Aubry, "Mode interaction models for near wall turbulence," J. Fluid Mech. **247**, 455 (1993).
[5]X. Zhou and L. Sirovich, "Coherence and chaos in a model of turbulent boundary layer," Phys. Fluids A **4**, 2855 (1992).
[6]G. Berkooz, P. Holmes, J. L. Lumley, N. Aubry, and E. Stone, "Observations regarding 'Coherence and chaos in a model of turbulent boundary layer' by X. Zhou and L. Sirovich [Phys. Fluids A **4**, 2855 (1992)]," Phys. Fluids **6**, 1574 (1994).
[7]L. Sirovich and X. Zhou, "Reply to 'Observations regarding 'Coherence and chaos in a model of turbulent boundary layer' by X. Zhou and L. Sirovich [Phys. Fluids A **4**, 2855 (1992)],' " Phys. Fluids **6**, 1579 (1994).
[8]U. Rist and H. Fasel, "Numerical simulation of controlled transition in a flat plate boundary layer," J. Fluid Mech. (in press).
[9]D. Rempfer and H. Fasel, "Evolution of three-dimensional coherent structures in a flat-plate boundary layer," J. Fluid Mech. **260**, 351 (1994).
[10]J. Guckenheimer and P. Holmes, *Nonlinear Oscillations, Dynamical Systems and Bifurcations of Vector Fields* (Springer, New York, 1983).
[11]E. Knobloch, M. R. E. Proctor, and N. O. Weiss, "Heteroclinic bifurcations in a simple model of double-diffusive convection," J. Fluid Mech. **239**, 273 (1992).
[12]B. Nicolaenko and Z.-S. She, "Symmetry-breaking homoclinic chaos and bursts in periodic Navier–Stokes flows," Eur. J. Mech. B/Fluids **10**, (suppl.), 67 (1991).
[13]A. Mahalov and S. Leibovich, "Weakly nonlinear analysis of rotating Hagen–Poiseuille flow," Eur. J. Mech. B/Fluids **10**, (suppl.), 55 (1991).
[14]P. S. Jang, D. J. Benney, and R. L. Gran, "On the origin of streamwise vortices in a turbulent boundary layer," J. Fluid Mech. **169**, 109 (1986).
[15]T. Herbert, "Secondary instability of boundary layers," Annu. Rev. Fluid Mech. **20**, 487 (1988).
[16]W. Koch, "On a degeneracy of temporal secondary instability modes in Blasius boundary-layer flow," J. Fluid Mech. **243**, 319 (1992).
[17]J. M. Rotenberry, "Finite amplitude steady waves in the Blasius boundary layer," Phys. Fluids A **5**, 1840 (1993).
[18]P. G. Saffman, "Vortices, stability and turbulence," Ann. N. Y. Acad. Sci. **404**, 12 (1983).
[19]A. C. Newell, D. A. Rand, and D. Russell, "Turbulent transport and the random occurrence of coherent events," Physica D **33**, 281 (1988).
[20]U. Ehrenstein, "Secondary bifurcations in plane Poiseuille flow with three interacting modes," Phys. Lett. A **186**, 403 (1994).
[21]F. P. Bertolotti, T. Herbert, and P. R. Spalart, "Linear and nonlinear stability of the Blasius boundary-layer," J. Fluid Mech. **242**, 441 (1992).
[22]U. Ehrenstein and W. Koch, "Three-dimensional wave-like equilibrium states in plane Poiseuille flow," J. Fluid Mech. **228**, 111 (1991).
[23]F. A. Milinazzo and P. G. Saffman, "Finite-amplitude steady waves in plane viscous shear flows," J. Fluid Mech. **160**, 281 (1985).
[24]W. Koch, "Strongly nonlinear oblique-wave solutions in wall-bounded shear flows," in *Nonlinear Instability of Nonparallel Flows*, edited by S. P. Lin, W. R. C. Phillips, and D. T. Valentine (Springer-Verlag, Berlin, 1994), pp. 117–126.
[25]J. D. Pugh and P. G. Saffman, "Two-dimensional superharmonic stability of finite amplitude waves in plane Poiseuille flow," J. Fluid Mech. **194**, 295 (1988).
[26]I. Soibelman and D. I. Meiron, "Finite amplitude bifurcations in plane Poiseuille flow: two-dimensional Hopf bifurcations," J. Fluid Mech. **224**, 197 (1991).
[27]J. Jiménez, "Bifurcations and bursting in two-dimensional Poiseuille flow," Phys. Fluids **30**, 3644 (1987).
[28]G. Iooss and D. D. Joseph, *Elementary Stability and Bifurcation Theory* (Springer, New York, 1980).
[29]D. Barkley, "Theory and predictions for finite-amplitude waves in two-dimensional plane Poiseuille flow," Phys. Fluids A **2**, 955 (1990).
[30]J. Carr, *Applications of Center Manifold Theory* (Springer, New York, 1981).
[31]G. Iooss and M. Adelmeyer, *Topics in Bifurcation Theory and Applications* (World Scientific, Singapore, 1992).
[32]E. Knobloch and M. R. E. Proctor, "Nonlinear periodic convection in double-diffusive systems," J. Fluid Mech. **108**, 291 (1981).
[33]H. B. Keller, "Numerical solution of bifurcation and nonlinear eigenvalue problems," in *Applications of Bifurcation Theory*, edited by P. H. Rabinowitz (Academic, New York, 1977), pp. 359–384.
[34]E. Stone and P. Holmes, "Noise induced intermittency in a model of a turbulent boundary layer," Physica D **37**, 20 (1989).
[35]S. Dhawan, "Direct measurements of skin friction," NACA Rep. No. 1121 (1953).
[36]M. Asai and M. Nishioka, "Development of wall turbulence in Blasius flow," in *Laminar–Turbulent Transition*, edited by D. Arnal and R. Michel (Springer-Verlag, Berlin, 1990), pp. 215–224.